

# The Transient Current Distributions in a Vertical Electrode and the Ground

Y. BECK<sup>±</sup> and A. BRAUNSTEIN<sup>Ψ</sup>

Electrical Engineering Faculty

<sup>±</sup>Holon Institute of Technology, <sup>Ψ</sup>Tel Aviv University

<sup>±</sup>52 Golumb st. Holon, <sup>Ψ</sup> Haim Levanon St. Tel Aviv

ISRAEL

<sup>±</sup>beck@hit.ac.il , <sup>Ψ</sup> aribraun@eng.tau.ac.il

*Abstract:* - This paper presents a model for calculating the transient space-time current distributions in vertical electrodes and to the surrounding ground. The model is based on the electromagnetic field theory for calculations of the step function wave-pair response. The method takes into account the parameters of the electrode, such as: the radius and the length of the electrode. Furthermore, the conductivity, permittivity and the propagation velocity of the currents in the ground are also considered. In the analysis, the electrode is divided into finite sections. Thereafter, the "Compensating Currents", ground leakage currents and the current in the electrode in each section are calculated at all times.

The model is applied by a MATLAB code for the calculations of the above-mentioned currents' distributions. The results show that for soils of high conductivity values, relative short electrodes are needed for dissipating transient currents such as lightning currents. Furthermore, soil conductivity is a more sensitive parameter compared to the radius of the electrode and the permittivity of the ground.

*Key-Words:* - Current distribution, Grounding electrodes Lightning, Transient response, vertical electrodes.

## 1 Introduction

The most important element in lightning protection systems is the grounding system. A good grounding system is the one which dissipates the lightning current efficiently into the ground [1]. For the design of optimal and effective grounding systems, better understanding of the behaviour of grounding systems under transient currents is essential. An optimal design is important for achieving Electromagnetic Compatibility (EMC) requirements, as well as good protection against high currents and voltage hazards [2].

Since the early twenties, researchers have dealt with various phenomena related to the response of grounding systems to transients with high amplitude currents and short rise times, such as the lightning phenomenon. Earlier, researchers with no available computers, made an effort to find analytical models only, [3-7]. Since the late seventies or early eighties, computers became more powerful and models tend to become numerical, [8-12]. Furthermore, some of the analytical formulations led to unsolvable equations, such as differential or integral equations, [13,14]. In recent years, such equations can be evaluated by numerical methods.

The majority of the papers in this field concentrate on the determination of either the Ground Potential Rise (GPR), or the transient impedance of the

lightning current (see for example Grcev and Popov (2005), [15]). The measurements and calculations of these parameters are an important factor for the design of substations in which equipment is located over the grounding grid. The information about the above mentioned GPR or the transient impedance is essential for the design of grounding electrodes and grids. The experiments for measuring these parameters are relatively simple, due to the fact that the measuring point is above ground level.

The knowledge of the current distributions in buried electrodes and the resulting leakage currents into the ground is essential for a better design of grounding systems. This analysis can improve the design of the electrodes shapes, grounding systems topologies, etc. There are only a few published papers which involve analysis of the current distribution and ground leakage currents in buried vertical electrodes.

In this paper, a model for calculating the response of a vertical electrode to a transient current is presented. The model is based on electromagnetic field theory, which is considered to be the most rigorous method for approaching the problem. The model takes into account the radius of the electrode and the conductivity and permittivity of the ground. The electrode is divided into finite sections. Thereafter, the "Compensating Currents", ground

leakage currents and the current in the electrode in each section are calculated at all times. The space-time distribution is also presented by taking into account the mutual effects of each segment.

Discretizing the electrode makes it natural to convert the analytical equations to computer based numerical expressions. The model is applied by a MATLAB code for the calculation of the above-mentioned current distributions. Studying the results of the simulation, yields to the conclusion that for soils of high conductivity values, relative short electrodes are required for the dissipation of the lightning current. Moreover, in low conductive soils there is no practical justification for the use of vertical electrodes. In this case, long horizontal electrodes are more efficient and recommended. Another observation is that soil conductivity is a more sensitive parameter compared to the radius of the electrode and the permittivity of the ground. This presented work offers an engineering tool for the assessment of the effective lengths of electrodes for various types of soils.

In this work the ionization phenomenon is neglected. This is justified due to the fact that in complicated and multiconductor grounding systems, the lightning current is divided between all conductors of the system. Thus, in most of the conductors and electrodes, ionization phenomenon will not occur.

## 2 The Wave Pair Model

### 2.1 The Horizontal NP Wave Pair Model

A theoretical model describing the incident transient current is based on the Wave Pair Model [4]. This model describes the lightning stroke based on electromagnetic wave propagation concept. Deriving the potential wave equation from Maxwell's equations yields:

$$\begin{aligned}\nabla^2 V - \frac{1}{c^2} \frac{\partial^2 V}{\partial t^2} &= -\frac{\rho}{\epsilon_0} \\ \nabla^2 \vec{A} - \frac{1}{c^2} \frac{\partial^2 \vec{A}}{\partial t^2} &= -\mu_0 \vec{J}\end{aligned}\quad (1)$$

When,  $V$  and  $\vec{A}$  are the scalar and vector potentials accordingly,  $\rho$  is the charge density and  $\vec{J}$  is the current density. These equations are valid only when the following condition (Loerenz Gauge condition) is fulfilled:

$$\nabla \cdot \vec{A} + \frac{1}{c^2} \frac{\partial V}{\partial t} = 0 \quad (2)$$

Due to symmetrical consideration the charge  $q$ , the charge per unit length, replaces  $\rho$ , and the current  $I$  replaces  $\vec{J}$ . The solution for the potentials  $V$  and  $\vec{A}$  introduced in Eq.1 is:

$$\begin{aligned}V &= \frac{1}{4\pi\epsilon_0} \int_s \frac{q(s; t - \frac{r}{c})}{r} \cdot ds \\ \vec{A} &= \frac{\mu_0}{4\pi} \int_s \frac{I(s; t - \frac{r}{c})}{r} \cdot d\vec{s}\end{aligned}\quad (3)$$

These are the well-known "retarded potentials".

The rotational Maxwell's equation for the electric field strength  $\vec{E}$  is:

$$\nabla \times \vec{E} = -\frac{\partial \vec{B}}{\partial t} \quad (4)$$

The vector potential  $\vec{A}$  is defined as:

$$\vec{B} = \nabla \times \vec{A} \quad (5)$$

From Eq. 4 and 5, it is obtained:

$$\vec{E} = -\nabla V - \frac{\partial \vec{A}}{\partial t} \quad (6)$$

(6) is used to calculate the electric field strength components at an observation point.

Calculating the potentials and the electric field strength due to a down going step function charge wave (see Fig.1) yields:

$$\begin{aligned}V &= 30I \frac{c}{v} \left[ \ln \left( U + \sqrt{U^2 + R^2} \right) - \ln \left( -\xi + \sqrt{\xi^2 + r^2} \right) \right] \\ \vec{A} &= 30I \frac{1}{v} \left[ \ln \left( U + \sqrt{U^2 + R^2} \right) - \ln \left( -\xi + \sqrt{\xi^2 + r^2} \right) \right] \cdot \hat{\xi}\end{aligned}\quad (7)$$

Where  $v$  is the velocity of the charge wave propagation,  $\xi$  and  $r$ , are the horizontal and vertical distances of the observation point from the origin,  $\hat{\xi}$  is a unit vector in the x-direction and the following definitions are used:

$$\begin{aligned}U &= \frac{c}{c+v} (vt - \xi) \\ R &= \sqrt{\frac{c-v}{c+v}} \cdot r\end{aligned}\quad (8)$$

Using (6) and (7) the horizontal and vertical components of the electric field strength can be obtained:

$$\vec{E}_x = 30I \frac{c}{v} \left[ \frac{\frac{c-v}{c}}{\sqrt{U^2 + R^2}} - \frac{1}{\sqrt{\xi^2 + r^2}} \right] \quad (9)$$

$$\vec{E}_y = 30I \frac{c}{v} \cdot \frac{1}{r} \left[ \frac{U}{\sqrt{U^2 + R^2}} + \frac{\xi}{\sqrt{\xi^2 + r^2}} \right]$$

Study, now the electric field strength components at an observation point  $P(\xi, r)$  due to a single step function charge wave, do not satisfy the condition of (2), which means that this configuration has no physical meaning. That is due to the fact that the source of the charge is not defined. Therefore, in order to be consistent with charge conservation and to avoid the necessity of defining the source. A wave pair – model was developed, as seen in Fig.1. [4]

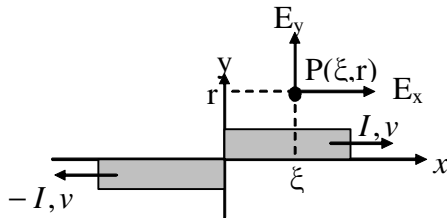


Fig.1: The opposite polarity two wave model

This model consists of two step functions. On the positive direction of axis  $x$  there is a positive polarity charge/current wave, traveling to the  $+x$  direction with velocity  $v$ . On the other direction there is a negative polarity charge/current wave traveling to the  $-x$  direction with the same velocity. This configuration is called PN (Positive Negative) wave-pair. The PN and the NP (Negative Positive, which is the complimentary configuration of the PN) configurations are the only ones that are with total agreement with the condition of (2).

Solving the potential equations for a NP or a PN model yields solutions which satisfy (2). These potentials are calculated in the same manner (7) was derived. Then, the potentials are substituted in (6) to obtain the electric field strength  $\vec{E}$  of an NP wave pair and the solutions are:

$$\vec{E}_x = 30I \frac{c}{v} \left[ \frac{c-v}{c} \left( \frac{1}{\sqrt{U_1^2 + R^2}} + \frac{1}{\sqrt{U_2^2 + R^2}} \right) - \frac{2}{\sqrt{\xi^2 + r^2}} \right] \quad (10)$$

$$\vec{E}_y = 30I \frac{c}{v} \cdot \frac{1}{r} \left[ \left( \frac{U_1}{\sqrt{U_1^2 + R^2}} - \frac{U_2}{\sqrt{U_2^2 + R^2}} \right) + 2 \frac{\xi}{\sqrt{\xi^2 + r^2}} \right]$$

where:

$$U_1 = \frac{c}{c+v} (vt - \xi)$$

$$U_2 = \frac{c}{c+v} (vt + \xi) \quad (11)$$

$$R = \sqrt{\frac{c-v}{c+v}} \cdot r$$

## 2.2 Asymmetric Orthogonal Current Wave Pair

An orthogonal current wave pair is a wave pair in which one current wave travels in one direction,  $\xi$ -axis for example, and the other one travels in a perpendicular direction to the first current wave ( $r$ -direction in Fig. 2). These wave pairs are useful for representing current waves in corners or dispersion of currents. The symmetric orthogonal wave pairs were described and dealt in [20].

Consider an asymmetric orthogonal current wave pair, shown in Fig. 2.

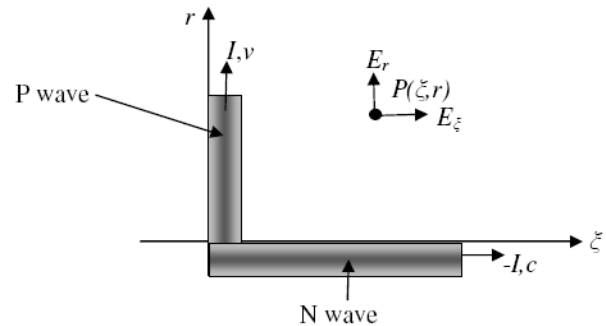


Fig.2: Asymmetric orthogonal current wave pair

This wave pair consists of a positive current wave with magnitude  $I$  traveling on the positive direction of the  $r$ -axis. This current travels at the velocity  $v$ . The other part of the current wave pair is a negative magnitude current wave ( $-I$ ), which travels in the positive direction of the  $\xi$ -axis. This wave is traveling at the velocity of  $c$ .

It is not yet obvious that the electric field strengths calculated at the observation point  $P(\xi, r)$  satisfy Lorentz's Gauge condition. Moreover, if the above-mentioned current wave does not satisfy that condition, it is physically unsound for use in the analytical model. The Scalar and Vector potentials,

due to such an orthogonal asymmetric current wave pair, need to be calculated at the observation point  $P(\xi, r)$ . Then the resulting potentials must be substituted and checked by the Lorentz Gauge Condition (2).

The scalar potential  $V$  and the vector potential  $\vec{A}$  for the N type wave traveling at the velocity of light  $c$  and the P type wave, traveling at constant velocity  $v$ , are:

$$\left. \begin{aligned} V_N|_{v=c} &= -30I \left[ \ln(ct - \xi) - \ln(-\xi + \sqrt{\xi^2 + r^2}) \right] \\ \vec{A}_N|_{v=c} &= -30I \frac{1}{c} \left[ \ln(ct - \xi) - \ln(-\xi + \sqrt{\xi^2 + r^2}) \right] \cdot \hat{\xi} \\ V_p &= 30I \frac{c}{v} \left[ \ln \left( U' + \sqrt{(U')^2 + (R')^2} \right) - \ln \left( -r - \sqrt{\xi^2 + r^2} \right) \right] \\ \vec{A}_p &= 30I \frac{1}{c} \left[ \ln \left( U' + \sqrt{(U')^2 + (R')^2} \right) - \ln \left( -r - \sqrt{\xi^2 + r^2} \right) \right] \cdot \hat{r} \end{aligned} \right\} \quad (12)$$

where:

$$\begin{aligned} U' &= \frac{c}{c+v} (vt - r) \\ R' &= \sqrt{\frac{c-v}{c+v}} \cdot \xi \end{aligned} \quad (13)$$

Substitution of the resulting potentials given by (12) into the Lorentz Gauge Condition (2) yields:

$$\begin{aligned} \nabla \cdot \vec{A} + \frac{1}{c^2} \frac{\partial V}{\partial t} &= -30I \frac{1}{c+v} \frac{1}{\sqrt{(U')^2 + (R')^2}} - 30I \frac{1}{c} \frac{1}{\xi - ct} + \\ &+ \frac{1}{c^2} \left[ 30I \frac{c^2}{c+v} \frac{1}{\sqrt{(U')^2 + (R')^2}} + 30Ic \frac{1}{\xi - ct} \right] = 0 \end{aligned} \quad (14)$$

Thus, the Lorentz-Gauge condition is satisfied and therefore the orthogonal asymmetric current wave pair is physically meaningful.

### 3 Description of the Model

The current distribution in the electrode and the ground leakage currents are studied. The model is based on the step function wave pairs described above. This model is applicable both for the current waves inside the electrode (conductor), as well as the ground currents (leaking from the surface of the electrode). The rectangularity of the current waves is kept by using the Compensating Currents theory [4].

For calculation of the currents, the electrode is divided into small segments,  $\Delta l$ . All segments are equal in length and considered small enough in a manner that the electric field is constant along  $\Delta l$ . A current, which propagates at the velocity of light, will cross a segment at  $t = \Delta l / c$ .

The method presented here is based on some assumptions, as follows:

- All electrode currents have axial components only.
- The net current is assumed to flow on symmetry axis of the conductor. Note that the conductor thickness is not neglected (the same as in thin wire approximation).
- The grounding electrode is made of a very good conducting material (perfect conductor).
- The radius of the electrode is much smaller than the buried length of the electrode.
- The soil is assumed to be a linear homogenous half space with conductivity  $\sigma$  and relative permittivity constant  $\epsilon_r$ .
- The soil is considered to be non magnetic with a relative permeability constant  $\mu_r = 1$ .
- The current flowing to the ground is perpendicular (the field is radial) to the surface of the electrode.
- The losses in the ground are much higher than in the conductor. Therefore, the skin effect in the conductor is neglected.
- The electrode is assumed to be a part of an effective grounding system. Consequently, the currents are low enough so that no ionization occurs.
- The ground leakage current is propagating at a constant velocity  $v$ . This velocity is determined by the ground relative dielectric parameter  $\epsilon_{gr}$ . The velocity is:  $v = c / \sqrt{\epsilon_{gr}}$ .
- The current in the electrode propagates at the velocity of light  $c$ .

#### 3.1 Calculations of the Currents in the First Segment

At  $t=0$ , an N-P current wave pair is injected into the origin of the electrode. This current is propagating at the velocity of light. Therefore, at  $t=t_1$ , the current and the following S.O.I (Sphere of Influence) will reach point no.1 on the symmetry axis of the electrode. In order to compensate for the axial electric field strength on the surface of the conductor (electrode), a P-N compensating current wave pair must be applied in point no.1. This compensating current is marked as seen in Fig.3.

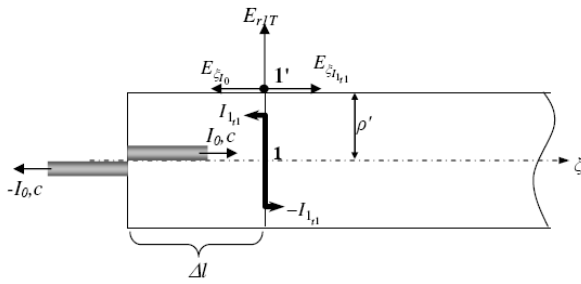


Fig.3: The electric fields and the compensating current at the first segment of the electrode  
The axial electric field strength due to  $I_0$  at the point no.1', located on the surface of the conductor, is:

$$E_{\xi_{I_0}} = 60I_0 \frac{1}{\sqrt{(\Delta l)^2 + \rho'^2}} \quad (15)$$

The electric field strength of the compensating current, located at point no.1 on the symmetry axis, is:

$$E_{\xi_{I_{l_{r1}}}} = 60I_{l_{r1}} \frac{1}{\rho'} \quad (16)$$

This compensating current compensates the axial field resulting from  $I_0$ . Therefore:

$$E_{\xi_{I_0}} = E_{\xi_{I_{l_{r1}}}} \quad (17)$$

then:

$$I_{l_{r1}} = I_0 \frac{\rho'}{\sqrt{(\Delta l)^2 + \rho'^2}} \quad (18)$$

Defining:

$$k_n = \frac{1}{\sqrt{(n \cdot \Delta l)^2 + \rho'^2}} \quad (19)$$

yields the expression for the first compensating current:

$$I_{l_{r1}} = k_1 I_0 \rho' \quad (20)$$

The perpendicular field strength at point no.1' is the sum of both normal fields at that point, resulting from  $I_0$  and  $I_{l_{r1}}$ . Since  $I_{l_{r1}}$  is located on the same  $\xi$  coordinate as point no.1' its contribution to the normal field is zero. Therefore, the resulting electric field strength in the  $r$  direction is:

$$E_{rT} = 60I_0 \frac{1}{\rho'} \frac{\Delta l}{\sqrt{(\Delta l)^2 + \rho'^2}} = 60I_0 \frac{\Delta l}{\rho'} k_1 \quad (21)$$

The surface of the electrode is assumed to be in direct contact with the ground. The ground is

assumed to be homogenous with conductivity  $\sigma$ . The current density at that point is then:

$$J = \sigma E_{rT} = 60I_0 \sigma \frac{\Delta l}{\rho'} k_1 \quad (22)$$

This density is equal for all points of the surface of the first segment (with length  $\Delta l$ ).

The resulting leakage current leaving the electrode towards the ground at that point is therefore the current density multiplied by the surface of a cylinder of length  $\Delta l$  and radius  $\rho'$ .

$$I_{g_{l_{r1}}} = 2\pi\rho' \cdot \Delta l \cdot \sigma \cdot 60I_0 \frac{\Delta l}{\rho'} k_1 = 120\pi\sigma \cdot \Delta l^2 I_0 k_1 \quad (23)$$

The ground leakage current  $I_{g_{l_{r1}}}$  is shown in Fig. 4 as a P-N wave pair (in order to satisfy the Lorentz Gauge Condition). The positive current of the wave pair is traveling perpendicular to the electrode's surface at a constant velocity  $v$ . The negative part of the wave pair is an axial current wave traveling on the symmetry axis of the electrode. In Fig. 4, the positive  $I_{g_{l_{r1}}}$  is shown on the surface of the electrode. However, it is assumed that the current wave is located at the symmetry axis of the conductor (see arrow in Fig. 4). This leakage current wave pair is different from  $I_0$  and  $I_{l_{r1}}$ , as the positive current is traveling at a constant speed  $v$  and the negative current is traveling at the velocity of light,  $c$ .

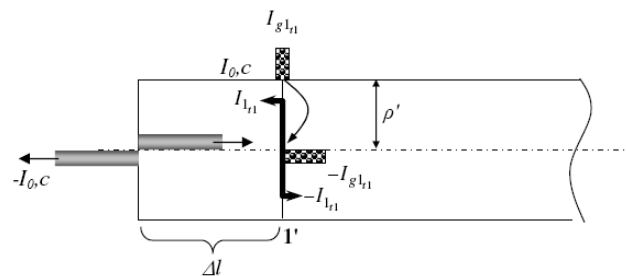


Fig.4: The resulting ground leakage current of the first segment of the electrode.

The initial current inside the electrode is  $I_0$  and it is fed at the origin of the electrode. When this current and its S.O.I passes point no.1', the current in the electrode is the sum of all currents which exist in the segment  $\Delta l$  between point no.1' and the next point (See Fig.5).

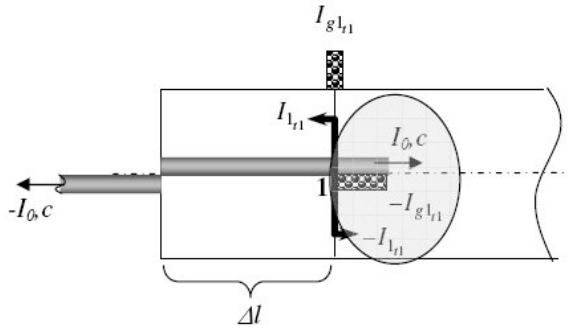


Fig.5: The current inside the electrode after the injected current passes point no.1

The sum of all the currents in the highlighted region in Fig.3 is:

$$I_{E1,1} = I_0 - I_{l1} - I_{gl1} \quad (24)$$

### 3.2 Calculations of the Currents in the Second Segment

At  $t = t_2 = 2 \cdot \Delta l / c$  the NP current wave pair ( $I_0$ ) and its S.O.I reaches point no.2. At this time, again, the axial electric field at point no.2' must be equal to zero. A new Compensating Current is formed at point no.2 (Fig.6).

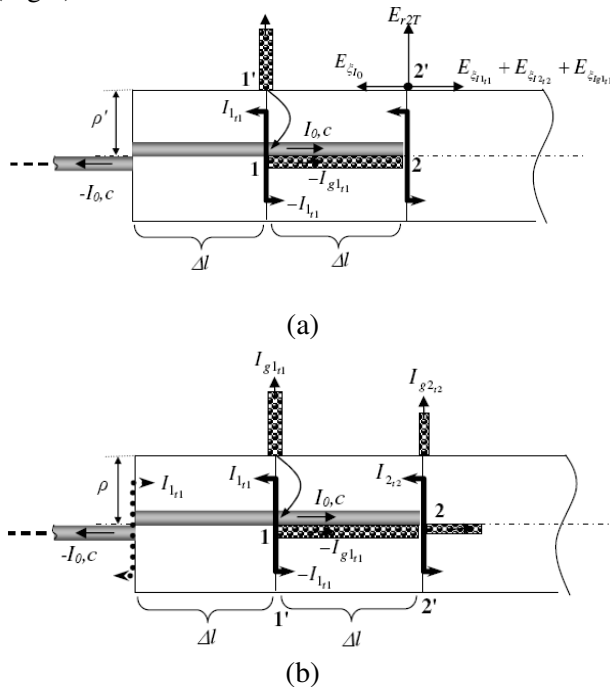


Fig.6: a) The electric fields, the compensating currents and ground currents, when the S.O.I due to  $I_0$  passed the second segment. b) All current waves

distribution existing when the S.O.I of  $I_0$  passed over the second segment

At point no.2', in addition to the second compensating current's axial field on the surface of the electrode, there is another axial field resulting from the new ground leakage current,  $I_{gl1}$ . The field of the injected current  $I_0$ , calculated at the point no.2' located at distance of  $2\Delta l$  from the origin, is:

$$E_{2\xi_{I_0}} = -60I_0 \frac{1}{\sqrt{(2 \cdot \Delta l)^2 + \rho'^2}} \quad (25)$$

The field of the first Compensating Current, located at distance of  $\Delta l$  from the point no.2, is:

$$E_{2\xi_{I_{l1}}} = 60I_{l1} \frac{1}{\sqrt{(\Delta l)^2 + \rho'^2}} \quad (26)$$

Another axial field originated from the ground leakage current is  $I_{gl1}$ . The axial field resulting from this current is:

$$E_{2\xi_{I_{gl1}}} = 30I_{gl1} \frac{c}{v} \frac{1}{\Delta l} \left[ \frac{U_1^t}{\sqrt{(U_1^t)^2 + (R_1^t)^2}} + \frac{\rho' + \Delta l \frac{v}{c}}{\sqrt{(\Delta l)^2 + \rho'^2}} \right] \quad (27)$$

where:

$$\left. \begin{aligned} U_n^t &= \frac{c}{c+v} \left( v \frac{n \cdot \Delta l}{c} - \rho' \right) \\ R_n^t &= \sqrt{\frac{c-v}{c+v}} \cdot n \cdot \Delta l \end{aligned} \right\} \quad (28)$$

The axial field in the equation, which balances the total axial field, is the axial field due to compensating current  $I_{2,2}$  at point no.2'. This field strength component is:

$$E_{\xi_{I_{2,2}}} = 60I_{l1} \frac{1}{\rho'} \quad (29)$$

Now the total axial components field equation can be written as:

$$\left. \begin{aligned}
 & E_{2\xi_{i0}} + E_{2\xi_{i_{l_1}}} + E_{2\xi_{i_{g_{l_1}}}} + E_{2\xi_{i_{2_2}}} = 0 \\
 & -60I_0 \frac{1}{\sqrt{(2 \cdot \Delta l)^2 + \rho'^2}} + 60I_{l_1} \frac{1}{\sqrt{(\Delta l)^2 + \rho'^2}} + \\
 & + 30I_{g_{l_1}} \frac{c}{v} \frac{1}{\Delta l} \left[ \frac{U_1'}{\sqrt{(U_1')^2 + (R')^2}} + \frac{\rho' + \Delta l \frac{v}{c}}{\sqrt{(\Delta l)^2 + \rho'^2}} \right] + \\
 & + 60I_{l_1} \frac{1}{\rho'} = 0
 \end{aligned} \right\} \quad (30)$$

The compensating current  $I_{2_2}$ , derived from (30) is:

$$\begin{aligned}
 I_{2_2} &= I_0 \rho' \cdot k_2 - I_{l_1} \rho' \cdot k_1 - \\
 & - \frac{1}{2} I_{g_{l_1}} \frac{c}{v} \frac{\rho'}{\Delta l} \left[ \frac{U_1'}{\sqrt{(U_1')^2 + (R')^2}} + \frac{\rho' + \Delta l \frac{v}{c}}{\sqrt{(\Delta l)^2 + \rho'^2}} + \left( \rho' + \Delta l \frac{v}{c} \right) k_1 \right]
 \end{aligned} \quad (31)$$

The vertical (r-direction) electric field can be calculated by the summing up of all electric fields in the r direction due to all abovementioned currents. The expression for this field is:

$$\left. \begin{aligned}
 & E_{2rT} = 60I_0 \frac{1}{\rho'} \frac{2 \cdot \Delta l}{\sqrt{(2 \cdot \Delta l)^2 + \rho'^2}} - 60I_{l_1} \frac{1}{\rho'} \frac{\Delta l}{\sqrt{(\Delta l)^2 + \rho'^2}} + \\
 & + 30I_{g_{l_1}} \frac{c}{v} \frac{1}{\rho'} \left[ \frac{c-v}{c} \frac{1}{\sqrt{(U_1')^2 + (R')^2}} - \frac{v}{c} - \frac{\rho' + \Delta l \frac{v}{c}}{\sqrt{(\Delta l)^2 + \rho'^2}} \right]
 \end{aligned} \right\} \quad (32)$$

Note that the perpendicular electric field strength of  $I_{2_2}$  at point no.2' is zero, as it was explained above for point no.1'. This perpendicular electric field will cause a ground leakage current whose magnitude is:

$$I_{g_{2_2}} = 2\pi\rho' \cdot \Delta l \cdot \sigma \cdot E_{2rT} \quad (33)$$

All current waves existing at this time are shown Fig.6-(b)

At  $t=t_2$ , the part of the PN compensating wave pair current  $I_{l_1}$  that flows to the left, reaches the end of the electrode and reflection occurs. The reflection is defined by the appearance of a new NP wave pair current with the same magnitude as  $I_{l_1}$  starting at the origin [4]. The left going part of the compensating current continues undisturbed on the symmetry axis of the electrode to its left side (see Fig.7).

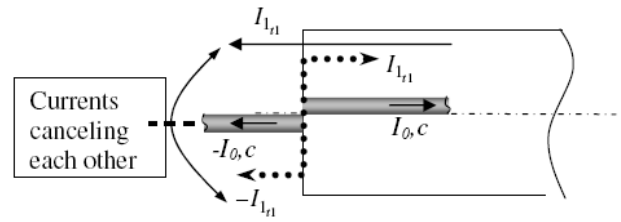


Fig.7: The currents of the model for a reflection at the origin of the electrode

The left going current wave of reflected Compensating Current is of a negative magnitude. Therefore it cancels the positive magnitude compensating current occupying the same fictitious conductor. Consequently, no current exists on the left of the electrode's origin. The currents on the right side of the origin do exist. Thus, the left going compensating current and the right going reflected compensating current continue as wave pairs. This procedure describes full reflection, without distortion of the wave pair model.

The current inside the electrode in the various sections can thus be calculated. The current of each section can be determined from the highlighted parts of Fig.8.

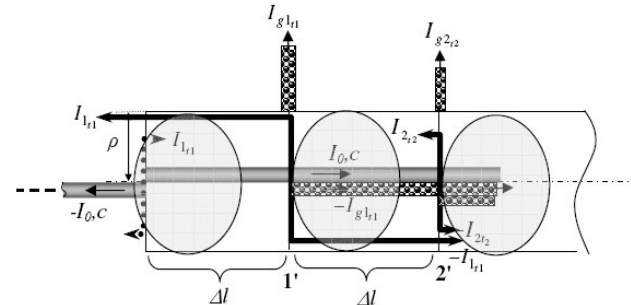


Fig.8: The currents inside the electrode after point no.2

At the origin, the electrode's current of the reflected compensating current is added to the injected current  $I_0$ . Thus the current is:

$$I_{E0_2} = I_0 + I_{l_1} \quad (34)$$

At the second segment after point no.2, the electrode's current is:

$$I_{E1_2} = I_0 - I_{l_1} - I_{g_{l_1}} \quad (35)$$

and at the third segment after point no.2, the current is:

$$I_{E2_2} = I_0 - I_{l_1} - I_{2_2} - I_{g_{l_1}} - I_{g_{2_2}} \quad (36)$$

(39)

### 3.3 Calculations of the Currents in the Third Segment

The same calculations are going to be repeated for the third segment (Fig.9). The reason for repeating the calculations is to underline the influence of the reflection phenomena which occurs at time  $t=t_2$ . The waves at  $t=t_3$  have reached point no.1 and the changes in the induced electric fields must be calculated. Therefore the currents  $I_{1,1}$  and  $I_{g1,1}$  must be re-valued.

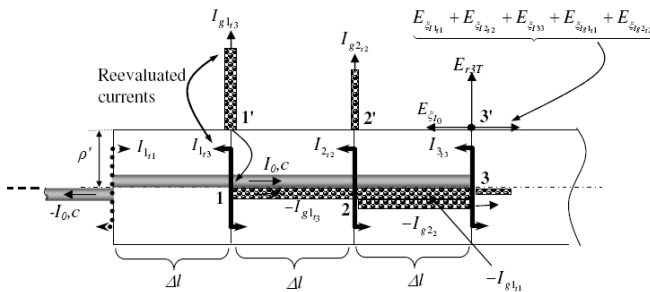


Fig.9: The currents at time  $t=t_3$  at points 1,2 and 3

$I_{1,3}$  can be derived from the axial field equilibrium as in (17) and (30) taking into account all the axial field influencing point 1'. Moreover, the perpendicular electric field at that point at time  $t=t_3$  yields the expression for the ground leakage current,  $I_{g1,3}$ . The re-evaluated currents at the end of the first segment at time  $t=t_3$  are then:

$$I_{1,3} = I_0 \rho' \cdot k_1 + I_{1,1} \rho' \cdot k_1 - I_{2,2} \rho' \cdot k_1 - \frac{1}{2} I_{g2,2} \frac{c \rho'}{v \Delta l} \left[ \frac{U_1^t}{\sqrt{(U_1^t)^2 + (R_1^t)^2}} + \left( \rho' - \Delta l \frac{v}{c} \right) k_1 \right] \quad (37)$$

and:

$$I_{g1,3} = 2\pi \rho' \cdot \Delta l \cdot \sigma \cdot E_{r1,3T} \quad (38)$$

where:

$$E_{r1,3T} = 60I_0 \frac{1}{\rho' \sqrt{(\Delta l)^2 + \rho'^2}} + \underbrace{60I_{1,1} \frac{1}{\rho' \sqrt{(\Delta l)^2 + \rho'^2}}}_{E_{r1,1} \text{ from reflected current}} - \underbrace{60I_{2,2} \frac{1}{\rho' \sqrt{(\Delta l)^2 + \rho'^2}}}_{E_{r2,2}} - 30I_{g2,2} \frac{c}{v \rho'} \left[ \frac{\frac{c-v}{c}}{\sqrt{(U^t)^2 + (R^t)^2}} - \frac{v}{c} - \frac{\rho' + \Delta l \frac{v}{c}}{\sqrt{(\Delta l)^2 + \rho'^2}} \right] \underbrace{\phantom{E_{r1,1} \text{ from reflected current}}}_{E_{r1,3T}}$$

The Compensating Current, the ground leakage current and the current inside the electrode at points 3 and 3' are calculated in the same manner, as described in the previous sections.

### 3.4. The Total Expressions for the Currents in all Sections at All Times

In the former sections, the various compensating ground leakage and conductor currents were studied. The Compensating Currents are the source for elimination of the axial electric field strengths on the surface of the electrode. The resulting Compensating Currents are used for calculation of the perpendicular electric field strengths directed towards the ground. After evaluating this field, the ground leakage currents were calculated, and then the current inside the electrode was also evaluated. This procedure has been done for three segments only in the electrode. Obviously, when the injected current propagates in the electrode, many more segments are involved and the amount of currents becomes enormous. Therefore, based on the currents calculated in the previous sections, it is possible to extend the calculations and define general expressions, which give the currents at any point in the electrode at any given time.

The general expression for the Compensating Currents distribution is:

$$I_{n_m} = \left\{ \begin{aligned} & \rho' k_n \left[ I_0 + \sum_{p=1}^{\frac{m-n}{2}} I_{p_{(m-n)-p}} \right] - \rho' \sum_{p=1}^{\frac{m-n}{2}} k_p I_{n+p_{m-p}} \\ & - \rho' \sum_{p=1}^{\frac{m-n}{2}} k_p I_{n-p_{m-p}} \\ & + \frac{1}{2} \rho' \frac{c}{v} \sum_{p=1}^{\frac{m-n}{2}} \frac{1}{p \cdot \Delta l} \left[ \frac{U_p'}{\sqrt{(U_p')^2 + (R_p')^2}} + \left( \rho' - p \cdot \Delta l \cdot \frac{v}{c} \right) k_p \right] I_{g_{n+p_{m-p}}} \\ & - \frac{1}{2} \rho' \frac{c}{v} \sum_{p=1}^{\frac{m-n}{2}} \frac{1}{p \cdot \Delta l} \left[ \frac{U_p'}{\sqrt{(U_p')^2 + (R_p')^2}} + \left( \rho' + p \cdot \Delta l \cdot \frac{v}{c} \right) k_p \right] I_{g_{n-p_{m-p}}} \end{aligned} \right\} \quad (40)$$

The general expression for the ground leakage current distribution is:

$$I_{g_{n_m}} = 2\pi\rho' \sigma \Delta l \left\{ \begin{aligned} & 60 \frac{n \cdot \Delta l}{\rho'} k_n \left[ I_0 + \sum_{p=1}^{\frac{m-n}{2}} I_{p_{(m-n)-p}} \right] \\ & - 60 \frac{1}{\rho'} \sum_{p=1}^{\frac{m-n}{2}} p \cdot \Delta l \cdot k_p \cdot I_{n-p_{m-p}} \\ & + 60 \frac{1}{\rho'} \sum_{p=1}^{\frac{m-n}{2}} p \cdot \Delta l \cdot k_p \cdot I_{n+p_{m-p}} \\ & + 30 \frac{c}{v} \frac{1}{\rho'} \sum_{p=1}^{\frac{m-n}{2}} \left[ \frac{\frac{c-v}{c} \rho'}{\sqrt{(U_p')^2 + (R_p')^2}} - \frac{v}{c} - \left( \rho' + p \cdot \Delta l \cdot \frac{v}{c} \right) \cdot k_p \right] \cdot I_{g_{n-p_{m-p}}} \\ & + 30 \frac{c}{v} \frac{1}{\rho'} \sum_{p=1}^{\frac{m-n}{2}} \left[ \frac{\frac{c-v}{c} \rho'}{\sqrt{(U_p')^2 + (R_p')^2}} - \frac{v}{c} + \left( \rho' - p \cdot \Delta l \cdot \frac{v}{c} \right) \cdot k_p \right] \cdot I_{g_{n+p_{m-p}}} \end{aligned} \right\} \quad (41)$$

and the general expression for the current inside the electrode is:

$$I_{En_m} = I_{E(n-1)I_m} - I_{n_m} - I_{gn_m} \quad (42)$$

In (42) the current at the origin must take into account all reflections. The expression for the edge conductor current is then:

$$I_{E0_m} = I_0 + \sum_{p=1}^{\frac{m}{2}} I_{p_{m-p}} \quad (43)$$

### 3.5 Matrix Representations of the Various Currents for MATLAB Programming

For calculation and presentation of the various currents distributions, a MATLAB Code was written. The program is used for the calculation of the Compensating Currents, the ground leakage currents and the current distribution, as summarized in (26)-(28).

In general, all currents are calculated at any point in time and space and a designated matrix is formed. Each matrix is a n-by-m matrix. The rows represent the position of the current on the axis of the electrode, or the position of the S.O.I on the surface

of the electrode (depending on the type of current). Each row is a sequential multiplication of an integer n (where n=1,2,3...) with the basic segment unit Δl. Thus, the rows represent the depth of the current propagation or the S.O.I propagation with respect to the origin of the electrode.

The columns are a representation of the time. This propagation time is calculated from the initial time t=t0, at which the injected current wave-pair starts. In the numerical process the time is assumed to be a discrete parameter, depending on the size of the segment unit Δl. The various currents time responses are calculated as discrete samples with a sample time, depending on the length of the electrode segment. As the currents in the electrode travel at a velocity of light, c, the time for the current to propagate at a distance of Δl is t = Δl/c. Therefore each column is a multiplication of an integer m (where m=1,2,3...) with the basic time sample Δl/c.

Thus, in all matrices, each component represents a current with space and time index. The general form of a matrix for any given current is:

$$I_{D_{n_m}} = \left\{ \begin{array}{cccccc} & & & \overbrace{\hspace{2cm}}^{m \cdot \frac{\Delta l}{c}} & & \\ & I_{D_{11}} & I_{D_{12}} & I_{D_{13}} & \cdots & \cdots & I_{D_{1m}} \\ 0 & & I_{D_{22}} & I_{D_{23}} & \cdots & \cdots & I_{D_{2m}} \\ 0 & 0 & & I_{D_{33}} & \cdots & \cdots & \vdots \\ \vdots & \vdots & & 0 & \ddots & & \vdots \\ \vdots & \vdots & \vdots & 0 & \ddots & & \vdots \\ 0 & \cdots & \cdots & \cdots & \cdots & 0 & I_{D_{nm}} \end{array} \right\} n \cdot \Delta l \quad (44)$$

where: D represents the type of current (Compensating Current, ground leakage current or the current in the electrode).

Study of the matrix of (44) yields that the matrix is an upper triangular one. This is due to the fact that at a certain depth in the electrode, where the S.O.I exists, the currents influence the fields of that point and the previous ones only. For example, when the S.O.I reaches the third segments (3 · Δl) at time t=t3, there are currents at the third, second and first segments only (see third row in the above matrix). For the calculation of the current inside the electrode a vector of the current at the injection point is added, following expression (43) as follows:

(45)

$$IOTm = [I_0, I_0, I_0 + I_{l_1}, I_0 + I_{l_1}, \dots, I_0 + \sum_{p=1}^m I_{pl_{m-p}}]$$

### 3 The Computer Simulation Results

#### 3.1 General

The Code was tested for many cases of various parameters. Each simulation was done for a different combination of conductivity  $\sigma$ , relative permittivity constant  $\epsilon_r$  and the radius of the electrode,  $\rho'$ . Since the discussed phenomenon is time dependant, it is important to note that each result shown in a graph describes a specific time only. The length  $\Delta l$ , is the calculation step of the algorithm. For smaller  $\Delta l$  the results are more accurate. The problem is that small calculation steps require more computer resources. Testing the codes for various values of  $\Delta l$  yields to the conclusion that choosing  $\Delta l$ , which is equal to the radius of the electrode, is sufficient (this result is also mentioned in Braunstein (1964) [4]).

#### 3.2 The Simulation Results

The model used here assumes that the ground is homogeneous. Thus the conductivity  $\sigma$  is obtained from geological research data [5]. The values of the conductivity vary between  $\sigma=0.2$  mho/m (resistivity of  $5\Omega/m$ ) for a conductive soil such as clay, up to  $\sigma=0.001$  mho/m for less conductive soil such as gravel.

In Fig. 10-(a) and (b), the resulting distributions of the current inside the electrode and the surrounding ground are presented. This is for the time in which the current propagated a distance of 3m along the vertical electrode. The electrode has a radius of 0.01m and is driven into a soil with a relative dielectric constant of 10. The graphs show the distributions for five resistivities (5, 10,100,500,1000 $\Omega m$ ). The injected current is a step function with a magnitude of 1A.

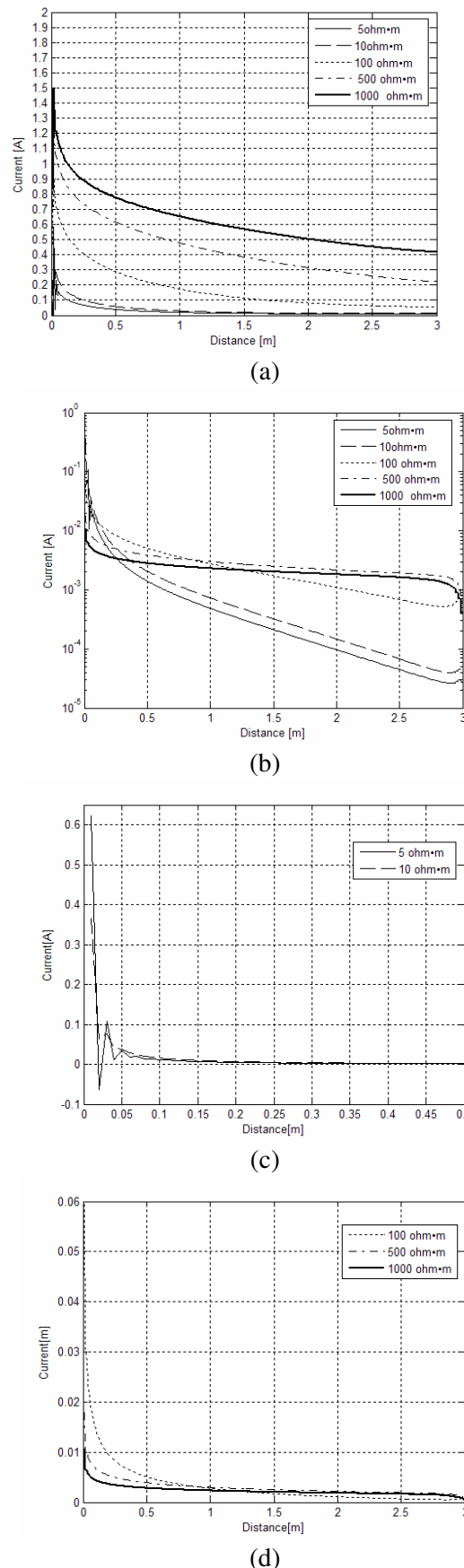


Fig. 10: Currents distributions for an electrode with radius of 0.01m driven into a soil with  $\epsilon_r=10$  for

various resistivities. a) The current distributions in the electrode. b) The current distribution in the surrounding ground. c) The current distribution in the surrounding ground for low resistivities. d) The current distribution in the surrounding ground for high resistivities.

The results presented in Fig. 10-(a) show that for low resistivities ( $5\Omega\text{m}$  and  $10\Omega\text{m}$ ), the current decays much faster than in the case of the higher resistivities. Moreover, the current reduces to less than 10% of its initial value after propagating a distance of 20-30cm in the lower resistivities ( $5\Omega\text{m}$  and  $10\Omega\text{m}$ ), a 1.5m at  $100\Omega\text{m}$  and it takes longer than 3m for the higher resistivities.

In Fig. 10-(b), the current distributions in the surrounding ground of the same electrode with the same conditions are presented. Again it is clear that the current distribution to the ground is better in the lower resistivities than in the higher ones. Since the axes are logarithmic it is difficult to get a clear vision of the characteristics of the current distributions at the various resistivities. Therefore, the distribution for the lower resistivities is shown in Fig. 10-(c) and for the higher ones is shown in Fig.10-(d).

Note that Fig. 10-(c) includes only 50cm of the electrode, while Fig. 10-(d) includes 3m. The results show that in low resistivities the current dissipates into the ground after 25-35cm, while in the higher resistivities after 3m, there is still current omitting into the ground.

A more vivid view is presented in the 2D and 3D examples of Fig.11-(a) and (b). Fig. 11-(a) shows the current distribution to the ground in the case of soil resistivity of  $5\Omega\text{m}$ . It is clear from this example that there is no current after 25cm, whereas Fig.11-(b) shows the current distribution to the ground in the case of soil resistivity of  $1000\Omega\text{m}$ . In this case not all the current dissipates to the ground even after 3m.

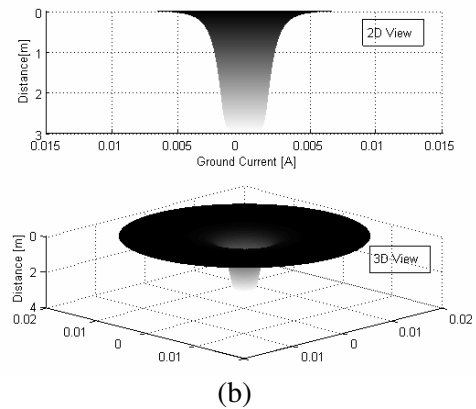
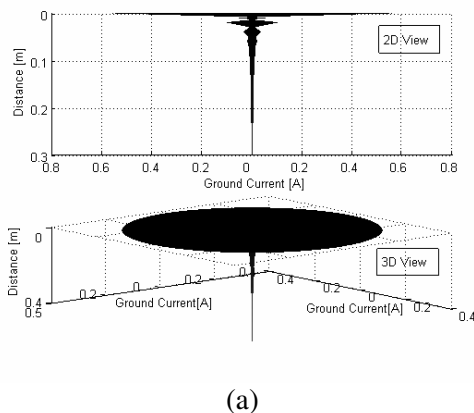


Fig. 11: a) 2D and 3D view of the current distribution in a soil with resistivity of  $5\Omega\text{m}$ . b) 2D and 3D view of the current distribution in a soil with resistivity of  $1000\Omega\text{m}$

Running the code for longer electrodes yields that in the case of high resistivity the current in the electrode decreases to about 10% of its initial value at a depth of about 13m.

The code was also tested for various radiuses and various relative dielectric constants. All the results show that the soil conductivity  $\sigma$ , is the most sensitive parameter.

## 4 Discussion and Conclusions

As mentioned above, the simulation results show that the soil conductivity  $\sigma$ , is the most sensitive parameter. Similar results are found also and reported [12], for the voltage change in grounding systems and in [16].

The results show that for soil with conductivity values higher than  $0.02[1/\Omega\text{m}]$ , 25cm effectively buried in the ground electrodes are sufficient. On the other hand, when soil conductivity is lower than  $0.001[1/\Omega\text{m}]$ , the length of electrodes may reach the length of 13m. This is in agreement with the results obtained by impedance calculations discussed in the work of Davis, Griffiths and Charlton [16] and [17]. The length of the electrode required by this study for soil conductivity value of  $0.001[1/\Omega\text{m}]$  is 13m and it agrees with the depth of the electrodes of 10-12m, as reported in these references, for the same conductivity [16],[17].

The results also show that in high conductive soils, the current dissipation is close to the ground level (very small depth). This effect was observed in many lightning strokes where top layers of the ground had traces of burns or are crystallized (see picture in [18]). The currents in these types of soils have higher magnitudes at depths close to the top edge of the electrode. This is in good agreement

with the calculated and measured results of ground potential of long horizontal buried electrodes, see for example Otero, Cidras and Alamo(1999), [19], Lorentzou and Hatziaargyriou(2000) [10] and Yaqing , Zitnik and Thottappillil(2001) [12]. The potentials reach higher values with a maximum close to the edge of the electrode. This means that higher currents must flow there in order to induce higher electric fields and higher potentials.

#### References:

- [1] Standard IEC 61312-1, *Protection Against LEMP; Part 1: General Principles*, 1995.
- [2] Markiewicz H and. Klajn A, *Earthing & EMC-Earthing Systems - Fundamentals of Calculation and Design, power quality application guide*, Leonardo Power Quality Initiative, June 2003.
- [3] Rubinstein M. and Uman M.A., Transient Electric and Magnetic Fields Associated with Establishing Finite Electrostatic Dipole, Revised, *IEEE Trans. on Elect. Compat.* Vol. 33, No. 4, pp. 312-320, Nov. 1991.
- [4] Braunstein A. , *Contribution to the Lightning Response of Power Transmission Lines*, Dr. Tech. Thesis, Chalmes University of Technology, Gothenburg, Sweden, 1964.
- [5] Sunde E.D., *Earth Conduction Effects in Transmission Systems*, Dover, New York, 1968.
- [6] Lundholm R., *Overvoltages in a Direct Lightning Stroke to a Transmission Line Tower*, CIGRE report No.333, Paris, 1958.
- [7] Wagner C.F., A New Approach to the Calculation of the Lightning Performance of Transmission Lines, Paper 56-733, *recom. By AIEE, Trans. And Dist. Comm. Presented at AIEE, Summer and Pacific General Meeting, San Francisco, Calif.*, 1956.
- [8] Loboda M. , Pochanke Z. , Current and Voltage Distribution in Earthing Systems, A Numerical Simulation Based on the Dynamic Model of Impulse Soil Conductivity, *20th ICLP, Switzerland*, September 24-28 , 1990.
- [9] Lorentzou M.I., Hatziaargyriou N., Modeling of Long Grounding Conductors Using EMTP, *IPST '99 - International Conference on Power Systems Transients*, Budapest, 20-24 June 1999.
- [10] Lorentzou M.I., Hatziaargyriou N.D., Effective Dimensioning of Extended Grounding Systems for Lightning Protection, *Proc. of the 25th ICLP Conference*, Rhodes, Greece. 18-22 Sept., 2000.
- [11] Lorentzou M.I., Hatziaargyriou N.D. and Papadias B.C., Time domain analysis of grounding electrodes impulse response, *IEEE Transactions on Power Delivery*, Vol. 18, Issue 2, pp. 517 – 524, April 2003.
- [12] Yaqing L., Zitnik M. and Thottappillil R., An Improved Transmission-Line Model of Grounding System, *IEEE Trans. on Elect. Compat.* Vol. 43, No. 3, pp. 348-355, August 2001.
- [13] Poljak D., Tham C.Y., *Integral Equation Techniques in Transient Electromagnetics*, Wit Press, 2003.
- [14] Poljak D., Doric V., Time Domain Modeling of Electromagnetic Field Coupling to Finite-Length Wires Embedded in a Dielectric Half Space, *IEEE Trans. on Elect. Compat.* Vol. 47, No. 2, May 2005.
- [15] Grcev L. , Popov M., On High Frequency Circuit Equivalents of Vertical Ground Rods, *IEEE trans. on Power Delivery*, Vol. 20, No. 2, April, 2005.
- [16] Griffiths H. and Davis A.M., Effective Length of Earth Electrodes Under High Frequency and Transient Conditions, *25th ICLP*, pp.469-473, Rhodes, Greece, 2000.
- [17] Davis A.M., Griffiths H. and Charlton T.E., High Frequency Performance of Vertical Earth Rod, *ICLP-98*, pp. 536-540, 1998.
- [18] Wang J., Liew A.C. and Darvenzia M., Extension of Dynamic Model of Impulse Behavior of Concentrated Grounds at High Currents, *IEEE Trans. on Power Delivery*, Vol. 20, No. 3, July 2005.
- [19] Otero A.F., Cidras J. and Alamo J.L., Frequency Dependant Grounding System Calculation by Means of a Conventional Nodal Analysis Technique, *IEEE Trans. on Power Delivery*, Vol. 14, No. 3, July 1999.
- [20] Berla D, *Induced Voltages in Loops due to Electromagnetic Fields Caused by Direct Lightning Stroke and Analysis of Protection Networks for Electrical and Electronics Systems*, PhD, Thesis, Tel Aviv University, 2003.